University of Sistan and Baluchestan

Chemical Process Design

Available online at http://cpd.usb.ac.ir/



Mitigation of Membrane Fouling in Microfiltration by Ozone Pretreatment: A Comparative Study on Flux Recovery, Fouling Reversibility, and Cake Layer Morphology

Mahdi Elyasi Kojabad[1]✉, Heidar Jafari[2]

[1] Corresponding Author, Department of Chemical Engineering, Faculty of Engineering, Behbahan Khatam Alanbia University of Technology, Behbahan, Iran. Email: m.elyasi@bkatu.ac.ir
[2] Persian Gulf Bidboland Gas Treating Company, Behbahan 63661-16314, Iran. Email: h.jafari@pgbidboland.ir

ARTICLE INFO

Article type: *Research Article*

Article history:
Received: 2026-05-17
Received in revised form: 2026-06-05
Accepted: 2026-07-12
Available online: 2026-07-12

Keywords: *Microfiltration; Membrane fouling; Ozonation; Ceramic membrane*

ABSTRACT

Membrane fouling remains the primary operational bottleneck limiting the efficiency of microfiltration (MF) processes in water treatment. This study introduces ozonation as a chemical pretreatment strategy to mitigate fouling in a custom-fabricated ceramic MF membrane. An alumina-based membrane with a peak pore size of 350 nm was successfully fabricated via gel-casting and characterized using FESEM and FTIR, revealing a homogeneous microstructure with a narrow pore size distribution. The integrated ozone-MF (O_3-MF) system was evaluated using surface water from the Maroon River. The membrane showed an initial pure water flux of 1100 $L.m^{-2}.h^{-1}$. In the absence of ozone, rapid and irreversible flux decline occurred, with hydraulic backwashing failing to restore performance. With ozone pretreatment, the membrane exhibited improved flux stability, achieving near-complete flux recovery after each backwash cycle. Based on these flux recovery data and visual observation of the membrane surface, ozonation appeared to alter the fouling layer characteristics, resulting in a less compact and more hydraulically reversible deposit compared to operation without ozone. The O_3-MF system also achieved 71% turbidity reduction, reduced total coliforms and E. coli to below the detection limit of the analytical method (<1.1 MPN/100 mL), and reduced the Silt Density Index (SDI) from 0.25 to below detectable limits, indicating improved effluent quality for downstream applications. These results suggest that the integration of ozonation with MF separation offers an effective low-pressure pretreatment strategy for enhancing membrane operational stability and reducing cleaning frequency.

Cite this article: Elyasi Kojabad, M., Jafari, H., (2027), Mitigation of Membrane Fouling in Microfiltration by Ozone Pretreatment: A Comparative Study on Flux Recovery, Fouling Reversibility, and Cake Layer Morphology, *Chemical Process Design*, 6(1), 1-14. http//doi.org/10.22111/cpd.2026.55413.1089

© The Author(s).
DOI: http//doi.org/10.22111/cpd.2026.55413.1089

Publisher: University of Sistan and Baluchestan.

ARTICLE IN PRESS

1. Introduction

Membrane fouling represents the single most persistent operational challenge limiting the widespread adoption of pressure-driven membrane processes in water treatment [1]. Regardless of the membrane pore size from reverse osmosis (RO) to microfiltration (MF) the deposition of colloidal particles, natural organic matter, microorganisms, and inorganic precipitates on membrane surfaces leads to declining permeate flux, increased energy consumption, frequent chemical cleaning, and shortened membrane service life [2, 3]. While much attention has been directed toward fouling in high-pressure RO systems due to their critical role in industrial water purification, Microfiltration membranes operating at significantly lower pressures are equally susceptible to fouling, particularly when treating surface waters with high loads of fine suspended solids and colloids [4]. Conventional strategies for MF fouling control rely primarily on hydraulic flushing, backwashing, and occasional chemical cleaning [5]. However, these approaches are inherently reactive rather than proactive, addressing the symptoms of fouling after it has already occurred. More critically, certain foulants particularly submicron colloids and hydrophobic organic matter adhere strongly to ceramic and polymeric membrane surfaces, forming compact, irreversible cake layers that hydraulic backwashing cannot effectively remove [6, 7]. Over successive filtration cycles, this irreversible fouling accumulates, necessitating increasingly aggressive chemical cleaning, which in turn degrades membrane materials and increases operational costs [8]. These limitations have motivated the development of chemical pretreatment strategies designed to modify foulant properties before they reach the membrane surface [9, 10]. Among these, ozonation has emerged as a particularly attractive option due to its strong oxidative capacity, rapid reaction kinetics, and absence of persistent chemical residues [11, 12]. When applied as a pretreatment prior to membrane filtration, ozone can induce several beneficial transformations in the feed water: (i) oxidation and partial mineralization of natural organic matter, reducing its fouling propensity; (ii) charge neutralization of colloidal particles, promoting their aggregation into larger, less pore-penetrating flocs; and (iii) inactivation of microorganisms, preventing biofilm formation on the membrane surface. These effects collectively alter the morphology and adhesion characteristics of the subsequent fouling layer, potentially converting it from a compact, irreversible deposit into a loose, hydraulically reversible cake [13, 14]. Despite the demonstrated promise of ozone-membrane hybrid systems, most existing studies have focused on integrating ozone with ultrafiltration (UF) or tighter membranes. Microfiltration (MF) operating with pore sizes typically between 100 nm and several micrometers offers distinct advantages for pretreatment applications, including higher permeate flux (reducing membrane area requirements) and lower transmembrane pressure. However, the coarser pore structure of MF membranes makes them more vulnerable to internal pore fouling and penetration of fine colloids unless effective pretreatment is provided. Ozonation, by aggregating submicron particles into larger flocs, is uniquely suited to bridge this gap: transforming feed water characteristics to match the separation capabilities of MF membranes. To date, systematic evaluations of ozone as a pretreatment specifically for ceramic MF membranes treating complex surface waters remain scarce. In particular, no studies have examined water from the Maroon River the feed source for the Bid Boland Persian Gulf Gas Refinery which carries a distinctive load of fine silt and colloidal materials derived from arid region geology. The composition of this water presents a unique fouling challenge that cannot be directly extrapolated from studies using synthetic waters or effluents from other geographical regions. In recent years, several recent investigations have explored ozone-based pretreatment in related contexts. Liu et al. (2024) demonstrated that softening coupled with ozonation effectively controlled RO membrane fouling in textile wastewater reclamation, although ozonation

ARTICLE IN PRESS

alone exacerbated fouling due to cation bridging effects. Wang et al. (2024) developed a catalytic ceramic membrane system with ozone micro-nano bubbles for treating RO concentrate, achieving efficient pollutant degradation and reduced fouling. While valuable, these studies focused on high-pressure RO systems or specialized waste streams, not on the specific objectives of enhancing MF performance for surface water pretreatment [17]. Therefore, the present study refocuses the inquiry from RO protection to a more fundamental question: can ozonation, as a chemical pretreatment, fundamentally alter fouling behavior in ceramic microfiltration? The specific objectives are: (i) to fabricate and characterize a ceramic MF membrane with controlled pore structure suitable for surface water treatment; (ii) to evaluate the impact of ozone pretreatment on MF permeate flux, fouling reversibility, and cake layer morphology; (iii) to quantify the improvements in effluent quality (turbidity, SDI, microbial indicators) achievable with the O_3-MF hybrid system; and (iv) to elucidate the mechanisms by which ozone transforms irreversible fouling into reversible fouling in MF processes. The findings provide a tailored evaluation of the O_3-MF pretreatment train for the specific water matrix of the Maroon River, offering an optimized solution to enhance MF operational stability and reduce cleaning frequency while producing high-quality effluent suitable for downstream applications, including reverse osmosis feed.

2. Materials and methods

2.1. Materials

Alumina powder (Al_2O_3, 96%, Khuzestan Refractory Co.) served as the base material. Sodium hydroxide (NaOH, 98%, Chlor Pars Co.) was used as a flux and pH regulator. For gel-casting, acrylamide (monomer, 99%), potassium persulfate (initiator, 99%), and di-ammonium phosphate (cross-linker, 99%) were supplied by Merck.

2.2. Fabrication of ceramic membranes and module assembly

The ceramic membranes were fabricated using a gel-casting method. To begin, acrylamide was dissolved in deionized water to form a monomer solution, and the pH was adjusted to 9 by adding 1 M NaOH. Alumina powder was then gradually incorporated into this solution, which already contained potassium metabisulfite as a reducing agent. The mixture was continuously stirred at 300 rpm for 48 hours to achieve complete homogenization. After this mixing period, the slurry temperature was elevated to 50°C, and di-ammonium phosphate was added as a cross-linking agent to initiate the polymerization reaction. The resulting slurry was poured into rectangular casting molds with internal dimensions of 10 cm × 30 cm × 1 cm (width × length × thickness). The molds were designed to produce flat-sheet membranes of uniform thickness. The cast slurry was then subjected to a controlled thermal treatment program. The first stage involved drying at 100°C for 2 hours to remove residual solvent and moisture. Subsequently, the dried green bodies were sintered at 1000°C for 3 hours. Both the heating and cooling ramps were precisely controlled at a rate of 5°C per minute. This controlled cooling rate was applied throughout the entire cooling phase from the peak sintering temperature down to ambient temperature, ensuring gradual thermal equilibration and preventing the development of thermal stresses or microcracks within the membrane structure. Following sintering, the fabricated flat-sheet membranes were assembled into filtration modules. A two-part epoxy adhesive with high bonding strength was used to pot the membranes inside custom-fabricated acrylic housings. The potting procedure was carried out using a precision mold-pouring technique to ensure complete isolation between the feed and permeate compartments. Specifically, the adhesive was carefully injected into the annular gap formed

ARTICLE IN PRESS

between the outer edge of the membrane and the inner wall of the housing, creating a leak-tight seal that prevents any unfiltered feed from bypassing the membrane and mixing with the permeate stream. Meticulous attention was devoted to eliminating any potential leakage paths that could lead to cross-contamination between the incoming raw water and the filtered product. After potting, the assembled modules were allowed to cure at room temperature for 24 hours, permitting the adhesive to fully harden and achieve its maximum sealing strength. Prior to any experimental runs, each module was subjected to integrity testing to verify the absence of leaks and to confirm proper hydraulic performance [18].

2.3. Hybrid Ozonation-MF System

A hybrid batch system was used (Fig. 1). High-purity oxygen (90-95%) from an oxygen concentrator was fed to a corona discharge ozone generator (1 g/h). The O_3/O_2 mixture was bubbled for 3 minutes into a 2.5 L glass reactor via a fine-pore diffuser. The injected ozone concentration was maintained at 20 mg/L. The ozonated water was directly fed to a filtration unit equipped with the fabricated ceramic membrane. The permeate flux (J) in liters per square meter per hour (LMH) was calculated using Eq. 1[19]:

$$J = \frac{V}{A.\Delta t} \tag{1}$$

Where V is the permeate volume (L), A is the effective membrane area (m^2), and Δt represents the filtration time interval (h).

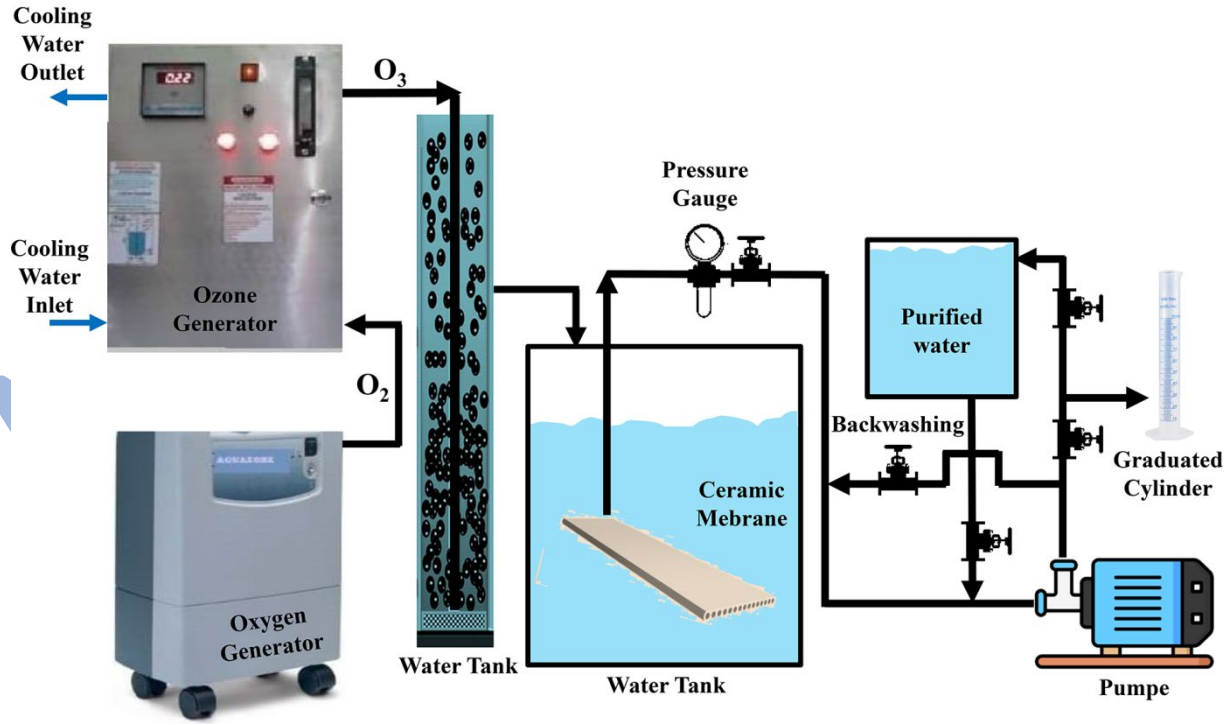


Fig. 1. Schematic illustration of the membrane filtration process

2.4. Characterization

Membrane morphology was analyzed by Field Emission Scanning Electron Microscopy (FESEM, MIRA3 FEG-

SEM, Tescan). Pore size distribution and density were determined from FESEM images using Digimizer software. Chemical functional groups were identified by Fourier Transform Infrared Spectroscopy (FTIR, Bruker alpha-p). XRD analysis was conducted on a Bruker D8 ADVANCE diffractometer (Cu-Kα, 40 kV, 40 mA), and contact angles were measured using a Jikan CAG-10 goniometer.

2.5. Water Quality Analysis

Water samples from different treatment stages were analyzed. Key parameters included turbidity (measured nephelometrically, NTU), Total Dissolved Solids (TDS, determined gravimetrically), and the Silt Density Index (SDI). The SDI was measured according to the ASTM D4189 standard method using a 0.45 µm microfilter membrane at a constant applied pressure of 30 psi. Total coliforms and E. coli were assessed using the multiple-tube fermentation technique, with results reported as MPN/100mL.

3. Results and Discussion

3.1 Surface morphology and pore structure

The surface topography and porous architecture of the sintered ceramic membrane were examined using FESEM. Three micrographs were captured at progressively increasing magnifications, labeled as Figs. 2a, 2b, and 2c, to provide a comprehensive view of the membrane's structural features across different scales. Fig. 2a presents a low-magnification overview of the membrane surface. This wide-field image reveals a noticeably uniform topography with no evidence of large-scale defects such as cracks, pinholes, or delaminated regions. The distribution of alumina particles across the surface appears highly consistent, indicating that the gel-casting and sintering procedures were successfully executed, yielding an intact and mechanically stable membrane layer.At intermediate magnification (Fig. 2b), the arrangement and packing behavior of individual Al_2O_3 grains become more discernible. The particles display predominantly angular to polyhedral geometries with a relatively narrow size range. These primary building blocks are tightly compacted against one another, creating an intricate three-dimensional network of interconnected solid phases. Evidence of successful sintering is clearly visible in the form of neck formation at particle-particle contact points, along with well-developed densified zones. The high-magnification image (Fig. 2c) offers a detailed view of the void spaces that constitute the filtration pathways. The interstitial gaps formed between adjacent sintered particles are irregular in shape yet remain interconnected throughout the structure, allowing fluid transport across the membrane thickness. These void dimensions fall within the nanometer scale, making the membrane suitable for rejecting fine colloidal matter and microorganisms. The manufacturing process yielded a relatively tight distribution of pore sizes, reflecting precise control over the fabrication parameters. Such a fine and uniform porous architecture is critical for achieving selective separation performance, particularly for the removal of suspended particulates, bacteria, and potentially viruses from aqueous streams [20]. These observations directly suggest the high efficiency of the prepared membrane in separation processes.

ARTICLE IN PRESS

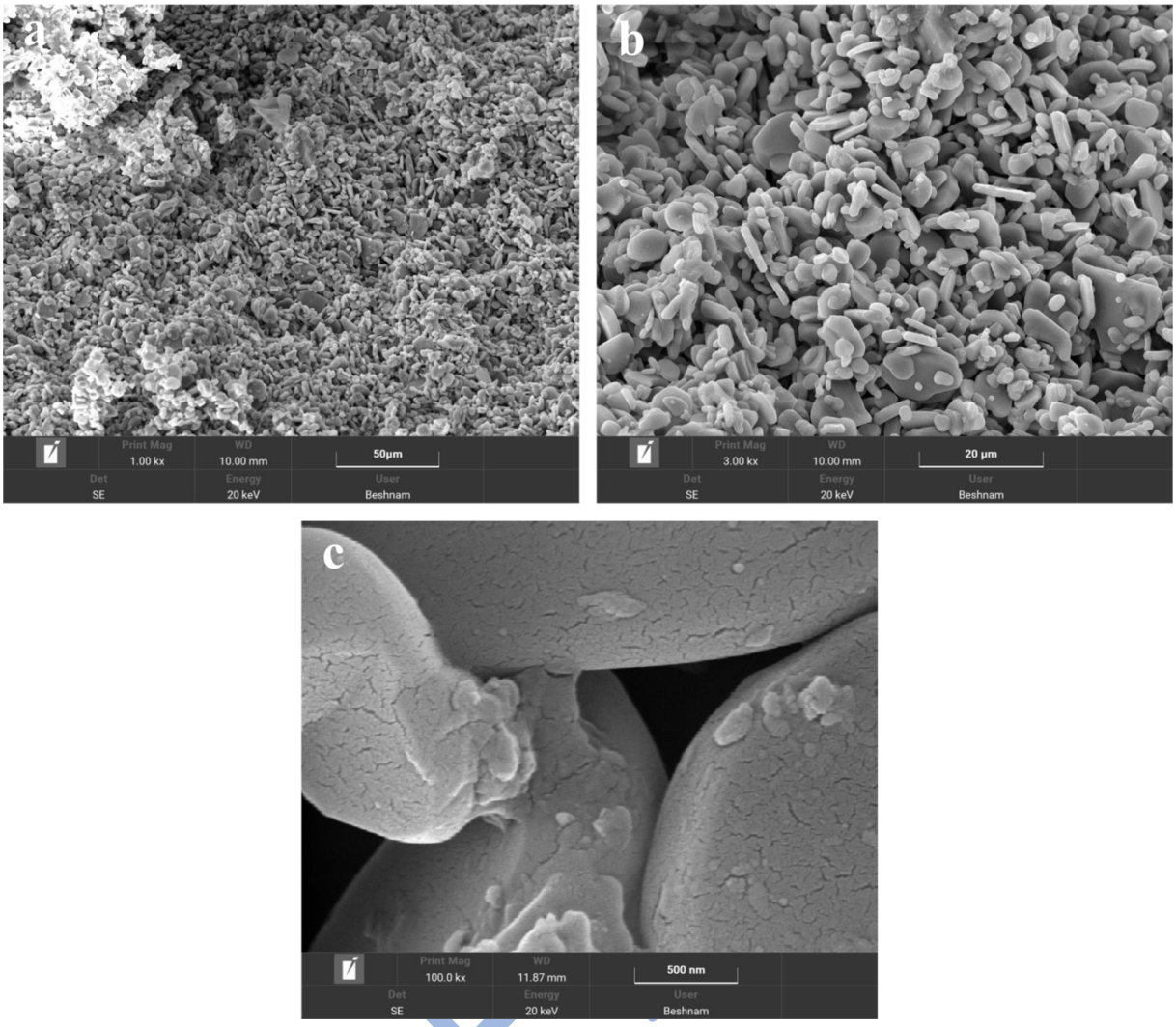


Fig. 2. FESEM micrographs of the fabricated ceramic membrane surface at different magnifications: (a) low magnification, (b) intermediate magnification, and (c) high magnification.

The pore diameter distribution of the fabricated membrane, derived from quantitative image analysis of the FESEM micrographs, is illustrated in Fig. 3. The histogram displays a unimodal pattern, with pore sizes predominantly concentrated within the range of approximately 50 to 850 nm. The distribution reaches its maximum frequency at a pore diameter of roughly 350 nm, indicating that this size occurs most abundantly across the membrane surface. The spread of the distribution is relatively confined, a feature typically associated with well-controlled sintering conditions and a homogeneous initial powder batch. Such uniformity is critically important for reliable separation performance, as it reduces the likelihood of oversized defects that could undermine rejection efficiency [21]. The vast majority of pores fall into a size category well-suited for retaining micron-scale particulates, colloidal matter, and microbial contaminants. Only a negligible fraction of pores appears at the extreme lower and upper ends of the size range, further attesting to the structural integrity and compositional consistency of the membrane layer.

ARTICLE

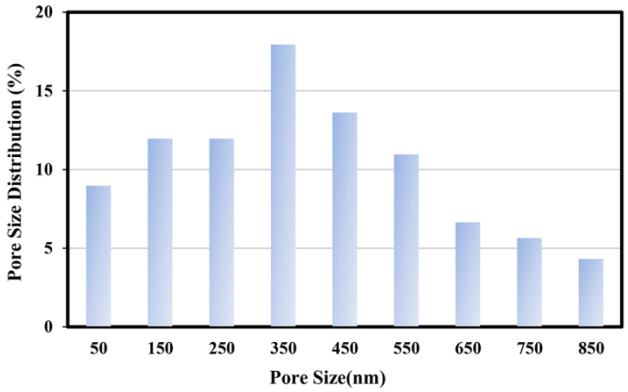


Fig. 3. Pore size distribution of the fabricated ceramic membrane derived from FESEM image analysis.

3.2 Crystalline structure and phase characterization

To verify the crystallographic identity and phase purity of the sintered ceramic membrane, XRD measurements were conducted. The resulting diffraction pattern, presented in Fig. 4, displays a series of sharp, well-resolved peaks characteristic of a highly ordered crystalline material. All observed reflections correspond precisely to the rhombohedral structure of α-alumina, commonly known as corundum. The distinctive diffraction signals appear at 2θ values of 25.6°, 35.1°, 37.8°, 43.4°, 52.6°, 57.5°, 66.5°, and 68.2°, which are assigned to the (012), (104), (110), (113), (024), (116), (214), and (300) crystallographic planes, respectively. Importantly, the diffraction pattern reveals no additional peaks that might indicate the presence of transitional alumina phases such as γ-Al_2O_3 or θ-Al_2O_3, nor any signals from unreacted starting materials. This absence confirms the high phase purity of the fabricated membrane. Furthermore, the pronounced intensity and narrow width of the diffraction peaks suggest a well-developed crystalline structure with a high degree of lattice order. The α-Al_2O_3 phase is particularly advantageous for membrane-based separation processes owing to its outstanding chemical inertness, robust mechanical properties, and excellent tolerance to aggressive cleaning agents and harsh operational environments. Collectively, the XRD findings, in conjunction with the FTIR spectroscopic data and FESEM morphological observations, provide unequivocal evidence that the fabricated membrane is composed of pure, highly crystalline α-Al_2O_3, possessing a stable and durable architecture well-suited for microfiltration applications.

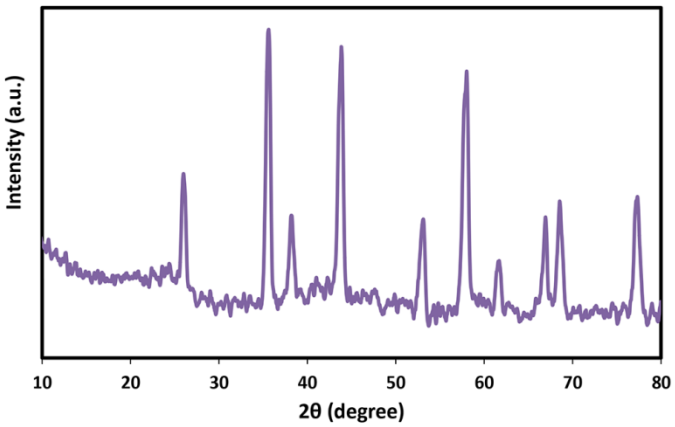


Fig. 4. X-ray diffraction pattern of the sintered alumina-based ceramic membrane.

ARTICLE IN PRESS

3.3 Chemical structure

Fourier Transform Infrared (FTIR) spectroscopy was utilized to characterize the surface chemistry of the fabricated ceramic membrane by identifying its functional groups and chemical bonds. The resulting spectrum, collected over a wavenumber range of 4000 to 400 cm^{-1}, is displayed in Fig. 5. The obtained spectral pattern exhibits features characteristic of alumina-based materials, providing confirmation that α-Al_2O_3 constitutes the dominant phase. A prominent broad absorption band appears between 3400 and 3450 cm^{-1}, which arises from O–H stretching vibrations of water molecules adsorbed onto the membrane surface. This observation is indicative of the highly hydrophilic nature of the fabricated membrane [22]. A weak H–O–H bending vibration appears near 1630 cm^{-1}, further supporting the hygroscopic nature of the alumina surface. Below 1000 cm^{-1}, the spectrum exhibits fundamental Al–O lattice vibrations. Broad absorption between 400 and 800 cm^{-1} is characteristic of Al–O stretching and bending in octahedral α-Al_2O_3. The features at 750 cm^{-1} and 580 cm^{-1} correspond to Al–O–Al bending, while the band at 450 cm^{-1} represents Al–O stretching. [23]. The lack of any sharp, isolated peaks in the spectrum and the presence of broad, merged bands are consistent with the polycrystalline and dense structure of the sintered alumina, as previously evidenced by the FESEM micrographs.

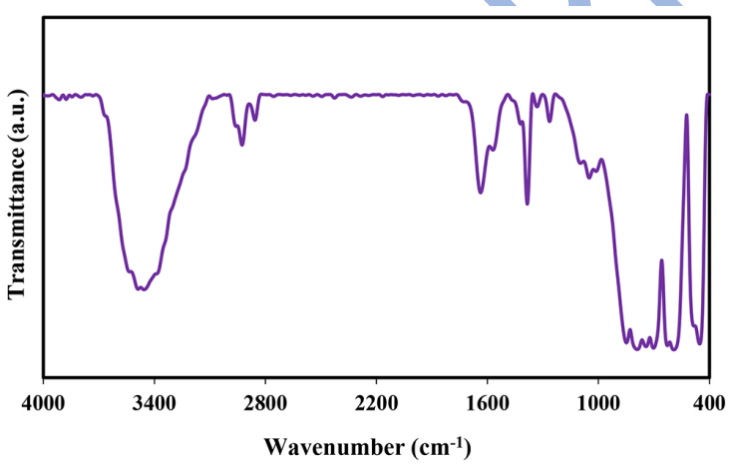


Fig. 5. FTIR spectrum of the prepared alumina ceramic membrane

3.4 Membrane Performance

The efficacy of the O_3-MF pretreatment in mitigating membrane fouling was unequivocally demonstrated through a comparative analysis of permeate flux profiles with and without ozonation, as shown in Fig. 6. In the baseline test without ozonation, the membrane experienced a severe and rapid decline in permeate flux. The initial flux of 1134 LMH plummeted to below 300 LMH within the first 780 seconds, indicating immediate and aggressive fouling. Subsequent hydraulic backwashing, performed at regular intervals, proved to be increasingly ineffective. The post-backwash flux recovery was minimal and exhibited a continuous downward trajectory (Fig. 6a). For instance, an early backwash at 660 seconds restored the flux to 603 LMH, but a later backwash at 1920 seconds only achieved a recovery to 85.7 LMH. This pattern signifies the rapid establishment of irreversible fouling, where deposited foulants form a compact, hydraulically resistant layer that cannot be removed by physical cleaning alone. By the end of the experiment, the flux stabilized at a critically low level near 89 LMH, underscoring a near-complete loss of membrane productivity. In stark contrast, the O3-MF process exhibited a remarkably stable flux profile. While a gradual decline was observed, the rate of flux reduction was significantly attenuated (Fig. 6b). More importantly,

the membrane demonstrated an exceptional response to backwashing. Each backwash event resulted in a near-complete recovery of the permeate flux, often returning it to values close to the initial flux (e.g., from 127.6 LMH to 900 LMH at 1460 seconds, and from 121.4 LMH to 391.3 LMH at 2510 seconds). This consistent and high level of flux recovery after each cleaning cycle is a clear indicator that the fouling layer formed in the presence of ozone is predominantly reversible. The fouling is likely loose, porous, and weakly adhered to the membrane surface, allowing it to be efficiently hydraulically removed. The visual evidence from the membrane autopsies provides profound corroboration for the flux data and offers critical insight into the fouling mechanisms at play (Fig. 7). The pristine, unused membrane exhibits a clean, white surface. The membrane subjected to ozonation prior to filtration retained a significantly cleaner appearance, with only minor, patchy discoloration. This suggests that the formed foulant cake layer was thin and non-uniform, consistent with the highly reversible fouling observed in the flux data. Conversely, the membrane used without ozonation was heavily fouled, displaying a thick, continuous, and dark-colored cake layer covering the entire surface. This dense layer acts as a secondary filtration barrier, increasing hydraulic resistance and leading to the severe flux decline observed. The visual evidence confirms that in the absence of ozone, colloidal particles, silt, and organic matter readily adsorb and accumulate on the membrane surface in a compact and sticky layer. The dramatic difference in performance can be attributed to the multifaceted role of ozone as a pretreatment agent. Ozone oxidizes natural organic matter (NOM) and neutralizes the surface charges of colloidal particles. This charge neutralization destabilizes the colloidal suspension, reducing electrostatic repulsion and promoting the aggregation of sub-micron particles into larger micro-flocs. These larger aggregates are less prone to penetrating and plugging membrane pores and form a more permeable, less resistant cake layer on the membrane surface. By oxidizing organic functional groups, ozone modifies the physicochemical properties of both the foulants and the membrane surface. This likely reduces the adhesion forces between the foulants and the membrane polymer, resulting in a cake layer that is more easily sheared off during cross-flow filtration and removed during backwash. While colloidal fouling is the primary focus, ozone's potent biocidal effect also inactivates bacteria, preventing the formation of biofilms that contribute to irreversible fouling.

ARTICLE IN PRESS

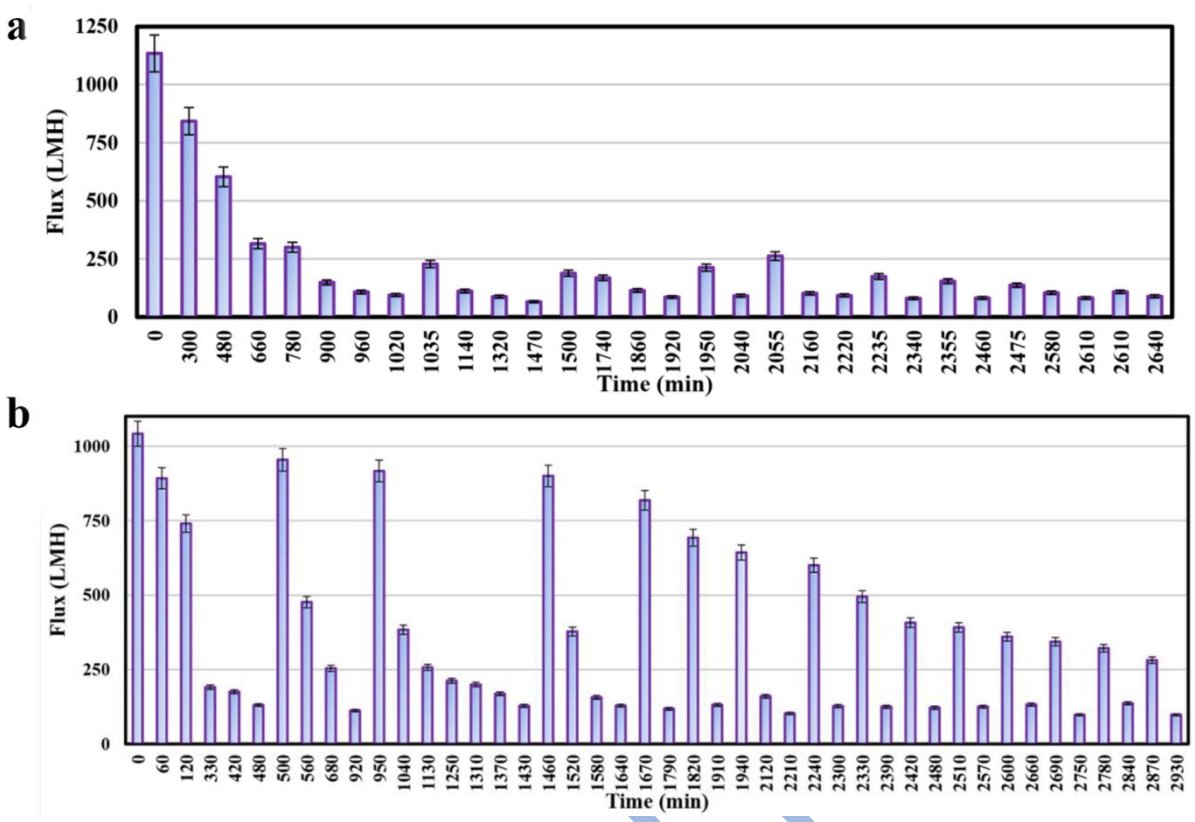


Fig. 6. Comparison of permeate flux during microfiltration cycles with periodic backwashing: bar chart showing flux values without ozonation (a) and with ozone pretreatment over time (b).

ARTICLE IN

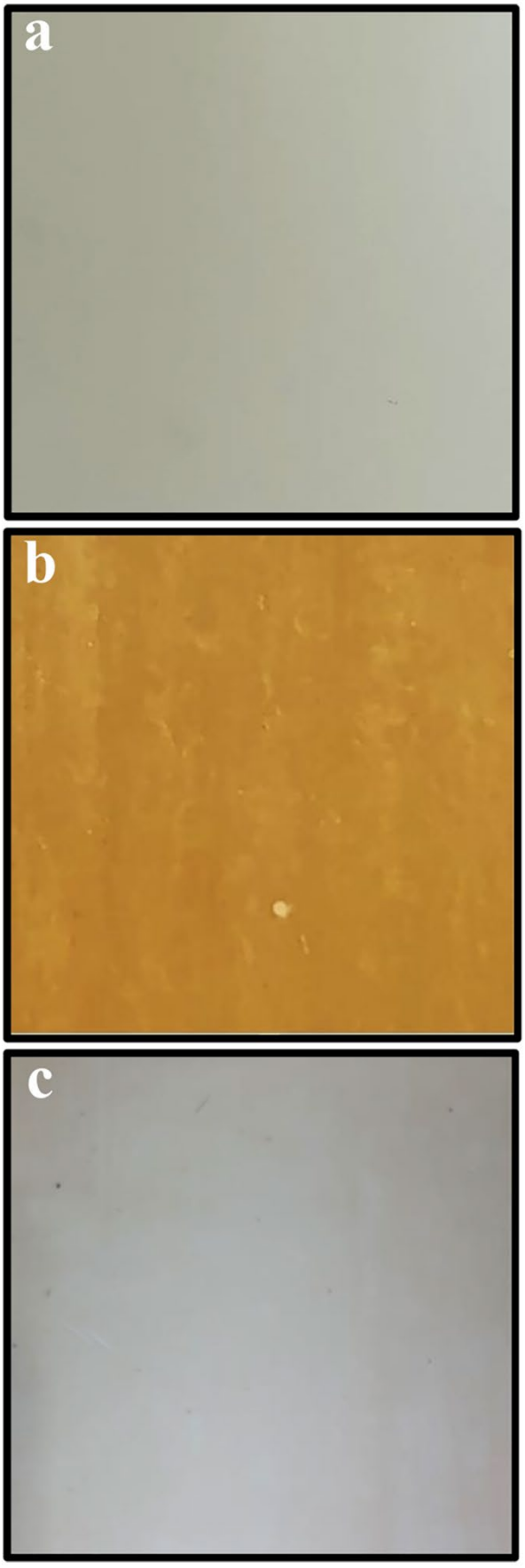


Fig. 7. Surface appearance of ceramic membranes under different operating conditions: (a) unused fresh membrane as a reference, (b) membrane subjected to filtration without ozonation, and (c) membrane subjected to filtration with ozone pretreatment.

3.5 Removal Efficiency and Colloidal Fouling

The effectiveness of the hybrid ozonation-MF system in controlling particulate and colloidal fouling was evaluated through systematic measurements of turbidity, TDS, and SDI. The results, summarized in Table 1, reveal outstanding performance of the combined treatment train in reducing physical fouling indicators. Feed water turbidity dropped from 1.72 NTU to 0.5 NTU after treatment, representing a removal rate of roughly 71%. This substantial reduction highlights the ability of the integrated setup especially the MF ceramic membrane to efficiently capture suspended solids and colloidal species that contribute to light scattering. In contrast, the TDS concentration remained constant at 1393.5 mg/L, an expected outcome given the pore size of the MF membrane. This unchanged TDS value clearly confirms that the dominant removal mechanism is physical sieving, which targets particulate matter while allowing dissolved ionic species to pass through unrestricted. The most compelling evidence of the pretreatment's efficacy is the dramatic decrease in SDI, falling from an initial value of 0.25 to below detectable limits. This substantial reduction indicates a decline in fouling potential by multiple orders of magnitude, reaching a level well below the stringent requirements typically specified for reverse osmosis membrane feed water.

Table 1. Comparison of TDS, turbidity, and Silt Density Index (SDI) values for raw water, ozonation-only effluent, and combined ozonation-microfiltration (O_3-MF) effluent

Sample	SDI	Turbidity (NTU)	TDS (mg/L)
Before treatment	0.25±0.01	1.72±0.95	1393.48±158.18
Ozone effluent	0.25±0.01	1.72±0.95	1393.48±158.18
Ozone-Membrane effluent	Below detectable limits	0.5±0.08	1393.48±158.18

3.6 Microbial Removal Efficiency

The microbial quality of water at different stages of treatment is summarized in Table 2. The raw water entering the system showed significant fecal contamination, with confirmed coliform and E. coli counts of 50 MPN/100 mL, clearly indicating the need for an effective disinfection barrier. Following ozonation alone, effective inactivation of microbiological indicators was observed, with both total coliforms and E. coli reduced to below detectable levels (<1.1 MPN/100 mL). This confirms the strong biocidal effect of ozone as a standalone treatment. The combined O_3-MF process likewise achieved effective removal of all target bacteria, with effluent values remaining below the detection limit of 1.1 MPN/100 mL. These results confirm that the hybrid O_3-MF system provides robust and reliable disinfection, ensuring microbial safety of the treated effluent. Unlike chemical disinfectants such as chlorine, ozone decomposes rapidly and does not leave persistent residues or generate significant amounts of harmful disinfection by-products. Thus, the synergistic O_3-MF process offers a sustainable and effective pretreatment strategy for producing microbiologically safe water suitable for downstream applications, including reverse osmosis feed [14, 24].

Table 2. Microbiological Analysis of Water Samples

Sample	Presumptive Coliform Count (MPN/100mL)	Confirmed Coliform Count (MPN/100mL)	E. coli (MPN/100mL)
Before treatment	110±10	60±10	60±10

ARTICLE IN PRESS

Membrane effluent	24±2	16±1	16±1
Ozone effluent	<1.1	<1.1	<1.1

4. Conclusion

This study comprehensively evaluated the efficacy of ozonation as a chemical pretreatment strategy for fouling control in a custom-fabricated alumina-based ceramic MF membrane. The results clearly demonstrate the positive synergy between ozone oxidation and MF separation. The hybrid O_3-MF system achieved effective performance in treating challenging surface water from the Maroon River. The most significant outcome was the fundamental transformation of fouling behavior induced by ozone pretreatment. In the absence of ozone, the MF membrane experienced rapid and severe flux decline, with hydraulic backwashing becoming progressively ineffective clear evidence of compact, irreversible cake layer formation. With ozone pretreatment, the membrane exhibited stable cyclic flux performance and near-complete flux recovery after each backwash cycle, demonstrating that the fouling layer had been converted from a compact, adherent deposit into a loose, hydraulically reversible one. This transformation was visually confirmed by membrane autopsy, which showed a substantially cleaner surface following O_3-MF filtration compared to the thick, dark cake layer observed without ozone. The O_3-MF system also produced exceptionally high-quality effluent. The SDI was reduced from 0.25 to below detectable limits, indicating substantial reduction of colloidal fouling potential. Turbidity was reduced by 71%, while TDS levels remained unchanged, confirming that the removal mechanism is physical sieving of particulate matter rather than rejection of dissolved species. Furthermore, the process provided complete disinfection, reducing total coliforms and E. coli from 50 MPN/100 mL to <1.1 MPN/100 mL, matching the performance of conventional chlorination without the associated risk of harmful disinfection by-products. Mechanistically, ozone pretreatment destabilizes colloidal suspensions through charge neutralization and oxidizes natural organic matter, promoting the aggregation of submicron particles into larger micro-flocs. These larger aggregates are less prone to pore penetration and form a more permeable, less adherent cake layer on the MF membrane surface. The result is a shift from irreversible fouling to reversible fouling, where the deposit can be efficiently removed by hydraulic backwashing. The integrated O_3-MF pretreatment system proves to be a highly effective, multi-barrier strategy for mitigating particulate, colloidal, and biological fouling in MF processes.

ARTICLE IN PRESS

Acknowledgements

The authors gratefully acknowledge the support provided by the Behbahan Khatam Alanbia University of Technology and the Persian Gulf Bidboland Gas Treating Company.

References

[1] Pepper, D., 1978. Reverse Osmosis and Ultrafiltration, no. 54, 117-121. https://doi.org/10.1007/978-3-642-67737-3_24.

[2] Fatima, S., Hashaikeh, R., Hilal, N., 2019. Reverse osmosis pretreatment technologies and future trends: A comprehensive review. Desalination, 452, 159-195. https://doi.org/10.1016/j.desal.2018.11.006

[3] Qaseem, M., Ahmad, S., Khan, M.Y., Akhtar, M.W., Ali, M.F., Ali, M.S., Ahmed, S., Bhutto, S., Altaf, M., 2025. Overview of sugar distillery wastewater characteristics and the potential of nanomaterial adsorbents for treatment in Sindh, Pakistan. Proceedings of the Pakistan Academy of Sciences: A. Physical and Computational Sciences, 62(3), 235-246. https://doi.org/10.53560/PPASA(62-3)702

[4] Elyasi Kojabad, M., Golizadeh kahnamouei, H., Babaluo, A.A., 2023. Investigation of the Structure and CO2/N2

Separation Performance of PEBA Membrane by Molecular Simulation Study. Chemical Process Design, 2(2), 37-41. https://doi.org/10.22111/cpd.2023.47331.1029

[5] Ye, H., Yan, Z., Lou, L., Sun, J., Zhong, J., Zhang, L., Liu, P., Feng, Z., 2026. Fouling in beer clarification using polyethersulfone hollow fiber membranes. Journal of Food Engineering, 406, 112823. https://doi.org/10.1016/j.jfoodeng.2025.112823

[6] Niebla, V. et al., 2025. Improved fouling resistance in polysulfone-based ultrafiltration membranes by the addition of polar peptoid oligomers obtained from Ugi-4CR. Synthesis and characterization. Polymer, 320, 1-14. https://doi.org/10.1016/j.polymer.2025.128090

[7] Shahcheraghi, N., Shafeei, S., Mostafaei, Z., Namjoufar, S., 2026. Advancements and applications of nanomembranes for wastewater treatment: A technical perspective. Journal of Applied Research in Water and Wastewater, 13(1), 1-10. https://doi.org/10.22125/arww.2026.481927.1301

[8] Yousefi, V., Mohebbi-Kalhori, D., Heydari, A., 2022. Milliliter-scale microbial fuel cell (MFC) fabricated by polyethersulfone (PES) hollow fiber membrane. Chemical Process Design, 1(2), 13-20. https://doi.org/10.22111/cpd.2022.43362.1005

[9] Anis, S.F., Hashaikeh, R., Hilal, N., 2019. Reverse osmosis pretreatment technologies and future trends: A comprehensive review. Desalination, 452, 159-195. https://doi.org/10.1016/J.DESAL.2018.11.006

[10] Ardeshiri Lordejani, H., Heidari, A., Ghods, N., 2022. Modeling of Sorkheh Reverse Osmosis (RO) Water Treatment Plant by Artificial Neural Network (ANN) with Genetic Algorithm (GA). Chemical Process Design, 1(1), 33-42. https://doi.org/10.22111/cpd.2022.43365.1006

[11] Foroughi, M., Khiadani, M., Kakhki, S., Kholghi, V., Naderi, K., Yektay, S., 2022. Effect of ozonation-based disinfection methods on the removal of antibiotic resistant bacteria and resistance genes (ARB/ARGs) in water and wastewater treatment: a systematic review. Science of the Total Environment, 811. https://doi.org/10.1016/j.scitotenv.2021.151404

[12] Kojabad, M.E., Aghdami, A., 2025. Investigating the effect of coagulation and ozonation on enhancing the efficacy of membrane filtration for papermaking effluent treatment. Iranian Wood and Paper Industries, 3. https://doi.org/10.22034/ijwp.2025.2045383.1687

[13] Kim, J., Fu, Q., Scofield, J.M.P., Kentish, S.E., Qiao, G.G., 2016. Ultra-thin film composite mixed matrix membranes incorporating iron(III)-dopamine nanoparticles for CO2 separation. Nanoscale, 8(15), 8312-8323. https://doi.org/10.1039/c5nr08840b

[14] Aghdami, A., Elyasi Kojabad, M., 2024. Wastewater Treatment Hybrid Process Using Coagulation-Membrane Filtration for Industrial Purposes. Applied Chemistry Today, 19(72), 269-282. https://doi.org/10.22075/chem.2024.33906.2267

[15] Liu, Y., Guo, Y., Yin, Z., Yang, W., 2024. Insights into coagulation, softening and ozonation pre-treatments for reverse osmosis membrane fouling control in reclamation of textile secondary effluent. Journal of Water Process Engineering, 58, 104764. https://doi.org/10.1016/j.jwpe.2023.104764

[16] Wang, S., Qiu, J., Ren, M., Cui, Y., Xie, Y., Cao, H., 2024. Enhanced treatment of reverse osmosis concentrates by ozone micro-nano bubbles coupled with catalytic ceramic membranes. Journal of Water Process Engineering, 61, 105213. https://doi.org/10.1016/j.jwpe.2024.105213

[17] Han, S.W., Kim, Y., Lee, K.H., Chae, S., 2025. Biomimetic piezocatalysts: A novel approach to water purification using TiO2/PVDF-TrFE. Results in Engineering, 28. https://doi.org/10.1016/j.rineng.2025.107438

[18] Mahdi Elyasi Kojabad, A.A., 2025. The treatment of papermaking effluent with the hybrid process of coagulation-ozonation-membrane filtration in order to recycle and reuse. Iranian Journal of Health and Environment, 18(2), 335-348. http://ijhe.tums.ac.ir/article-1-7010-fa.html

[19] Fu, W. et al., 2023. Nano-ceramic membranes combined with ozonation for water treatment: Fundamentals and engineering applications. Journal of Hazardous Materials Advances, 10. https://doi.org/10.1016/j.hazadv.2023.100279

[20] Ebrahimi, M., Busse, N., Kerker, S., Schmitz, O., Hilpert, M., Czermak, P., 2015. Treatment of the bleaching effluent from sulfite pulp production by ceramic membrane filtration. Membranes, 6(1), 7. https://doi.org/10.3390/membranes6010007

[21] Behboudi, A., Jafarzadeh, Y., Yegani, R., 2017. Polyvinyl chloride/polycarbonate blend ultrafiltration membranes for water treatment. Journal of Membrane Science, 534, 18-24. https://doi.org/10.1016/j.memsci.2017.04.011

[22] Kojabad, M.E., Bekhradinassab, E., Kahnamouei, H.G., 2024. Reinforced facilitated transport PEBA membrane by 2D Fe-doped TiO2 macroporous nanosheets for CO2 separation: Utilizing cationic and non-ionic surfactants. Journal of Environmental Chemical Engineering, 12(5), 113963. https://doi.org/10.1016/j.jece.2024.113963

[23] Kojabad, M.E., Amirabedi, P., Dorfeshan, M., 2024. A Two-Way Facilitated Transport Membrane for CO2 Separation with Synergy of Nucleophilic Addition and Π-Complexing Reactions: Molecular Simulation and Experimental Study, 36(6), 647-660. https://doi.org/10.22063/JIPST.2024.3470.2258

[24] Zare, J., Abbasi, M., Hashemifard, S.A., Khosravi, A., 2023. Coalescence Process: An Optimal and Economical Solution for Offshore Produced Water Treatment. Chemical Process Design, 2(2), 42-51. https://doi.org/10.22111/cpd.2023.45601.1020

ARTICLE IN PRESS